Available online at www.sciencedirect.com
ScienceDirect
European Journal of Medicinal Chemistry 44 (2009) 511–518
EUROPEAN JOURNAL OF MEDICINAL CHEMISTRY
http://www.elsevier.com/locate/ejmech

Original article

Synthesis and biological evaluation of a new family of *anti*-benzylanilinosulfonamides as CA IX inhibitors

Anne Thiry [a,*,1], Aurélie Delayen [b,1], Laurence Goossens [b], Raymond Houssin [b], Marie Ledecq [a], Aurélie Frankart [a], Jean-Michel Dogné [a], Johan Wouters [a], Claudiu T. Supuran [c], Jean-Pierre Hénichart [b], Bernard Masereel [a]

[a] *Drug Design and Discovery Center, FUNDP, University of Namur, 61 rue de Bruxelles, 5000 Namur, Belgium*
[b] *Institut de Chimie Pharmaceutique Albert Lespagnol, EA 2692, Université de Lille 2, 3 rue du Professeur Laguesse, BP 83, 59006 Lille, France*
[c] *Polo Scientifico, Laboratorio di Chimica Bioinorganica, Rm. 188, Università degli Studi di Firenze, via della Lastruccia 3, 50019 Sesto Fiorentino, Florence, Italy*

Received 1 February 2008; received in revised form 27 March 2008; accepted 27 March 2008
Available online 4 April 2008

Abstract

We report the synthesis and the pharmacological evaluation of a new class of human carbonic anhydrase (hCA) inhibitors prepared regio- and stereoselectively by reacting sulfanilamide with ethyl *trans*-phenylglycidate in the presence of cobalt(II) chloride. Various derivatizations of the ester moiety in the parent compound led to a small library of derivatives (2*R*,3*R* and 2*S*,3*S*) which displayed interesting inhibitory activities towards the human tumor-associated isoform CA IX. One of the new compounds shows high selectivity in inhibiting hCA IX compared to the two physiologically relevant, cytosolic isozymes hCA I and hCA II. A molecular modeling study was conducted in order to simulate the binding mode of this new family of enzyme inhibitors within the active sites of hCA IX and hCA II.

Keywords: Carbonic anhydrase; Tumor-associated isoform; Sulfonamide; Molecular modeling

1. Introduction

Human carbonic anhydrase IX (hCA IX) is overexpressed in many cancer tissues, when compared to its presence in normal, non-tumor cells. hCA IX has been shown to acidify the extracellular medium, contributing to the acquisition of metastatic phenotypes and creating chemoresistance to weakly basic anticancer drugs. This constitutes therefore an interesting target for novel approaches to anticancer therapy [1,2]. Classical hCA inhibitors already described are characterized by the presence of aromatic or heterocyclic sulfonamide/sulfamate/sulfamide scaffolds [3,4].

More generally, CA inhibitors (CAIs) have clinical applications such as anti-glaucoma, anti-obesity, anti-epileptic [5] and/or anti-tumor drugs/diagnostic agents [1–7]. It is obvious that different isozymes of the 16 presently known in mammals are preferentially targeted by various compounds with different pharmacological activity: anti-glaucoma drugs primarily target CA II, CA IV and probably CA XII, anti-obesity compounds the mitochondrial isoforms CA VA and CA VB, the anti-epileptic derivatives CA VII and CA XIV [5], whereas the anti-tumor derivatives target the transmembrane, tumor-associated isoforms CA IX and CA XII which are highly overexpressed in many types of hypoxic tumors [1,2].

We describe here the synthesis and screening of new sulfonamides as possible CAIs, in the search for derivatives with selectivity towards the tumor CA isozyme over cytosolic CA isozymes. Several original compounds were prepared and tested towards tumor-associated hCA IX and towards two

* Corresponding author. Tel.: +32 (0) 81 72 42 91; fax: +32 (0) 81 72 42 99.
E-mail address: anne.thiry@fundp.ac.be (A. Thiry).
[1] A.T. and A.D. equally contributed to this work.

0223-5234/$ - see front matter © 2008 Elsevier Masson SAS. All rights reserved.
doi:10.1016/j.ejmech.2008.03.034

other biologically relevant hCA isozymes, the ubiquitous, cytosolic, hCA I and hCA II. In order to rationalize the structure–activity relationships, docking simulations inside the previously designed model of hCA IX [8] and the crystallographic structure of hCA II were performed and compared with what is shown here to be the most interesting candidate.

2. Results and discussion

2.1. Chemistry

The compounds designed in the present work are shown in Chart 1. The current method to prepare 1,2-amino alcohols is represented by the nucleophilic ring opening of epoxides by amines. A regiocontrolled ring opening of epoxides has previously been described through a metal-assisted chelating process in an aprotic solvent [9]. When lithium methodology was applied (LiI or $LiClO_4$, acetonitrile), the reaction was effective (80% yield) if aniline was devoid of a sulfonamide or methylsulfone group, probably because in this case the Lewis acid character of the metal was not masked by a preferential chelation with one SO_2 oxygen.

The target parent compound **1** (Scheme 1) was efficiently prepared in a regio- [10] and stereoselective [11] manner by reacting 4-aminobenzenesulfonamide (sulfanilamide) with ethyl *trans*-phenylglycidate in the presence of a catalytic amount of cobalt(II) chloride; the moderate yield observed here (56%) is explained by the lower nucleophilicity of the amino group caused by the strong deactivation created by the sulfonamido group. This reaction induced aminolysis of the ester function as well as the formation of the expected amino alcohol **1**, whatever the solvent, stoichiometry of reactants or temperature. The *anti* stereochemistry of enantiomeric amino alcohols **1** was supported by the ^1H NMR chemical shift ($\delta < 5$ ppm) of the *N*-methine proton (previously established by X-ray data [12]) and was preserved for amino alcohols **2**–**5**. Hydroxamate **2** was obtained by treating ester **1** with hydroxylamine [13], whereas carboxylic acid **3** and primary alcohol **4** were obtained by hydrolysis (ethanolic sodium hydroxide) or by reduction ($LiBH_4$), respectively. Benzyl ether **5** was prepared from **1** by etherification (benzyl bromide, potassium carbonate) and subsequent reduction of ester **6** with $LiBH_4$.

2.2. CA inhibition

The CA inhibitory activity of compounds **1**–**5** is presented in Table 1. Data for acetazolamide (AZA), a clinically used hCA inhibitor, are quoted for comparison. Selective inhibitors of the hCA IX isozyme can be indicated with K_I ratios of hCA I over hCA IX, and hCA II over hCA IX. From these results, the inhibition pattern towards hCA I is obviously rather different from that of hCA II and hCA IX. This feature could be explained by the topology of the hCA I active site which is restrained by the presence of additional histidine residues [3]. The compounds studied here exhibit weak inhibition to hCA I, except for compound **2** which possesses a hydroxamate side chain (CONHOH) thought to be favorable to the inhibition of the isozyme hCA I ($K_I = 62$ nM).

Inhibitory activities towards the physiologically relevant isozyme hCA II ranged from 1.4 nM for the most active molecule (hydroxamate **2**) to 91 nM (benzyl ether **5**). The inhibition profile with regard to hCA IX exhibits K_I within the same range (1.8–227 nM). All inhibitors, except benzyl ether **5**, are selective towards hCA IX vs. hCA I. The highest selectivity for hCA IX vs. hCA II is observed for carboxylic acid **3** which is also the most potent hCA IX inhibitor.

2.3. Docking studies

Characterization and comparison of the active sites of the hCA II and hCA IX isoforms have already been described

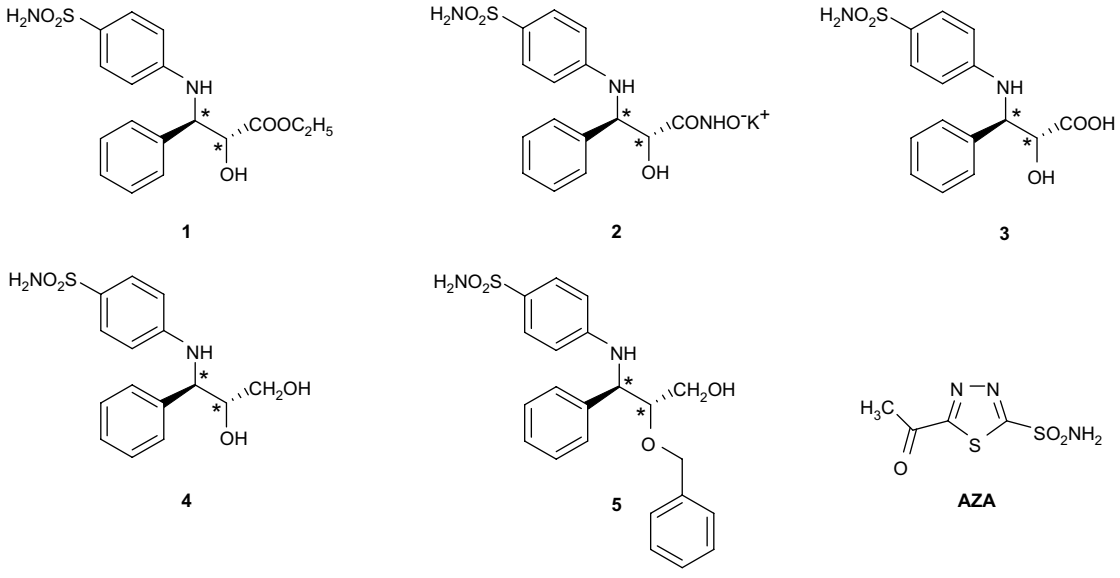

Chart 1.

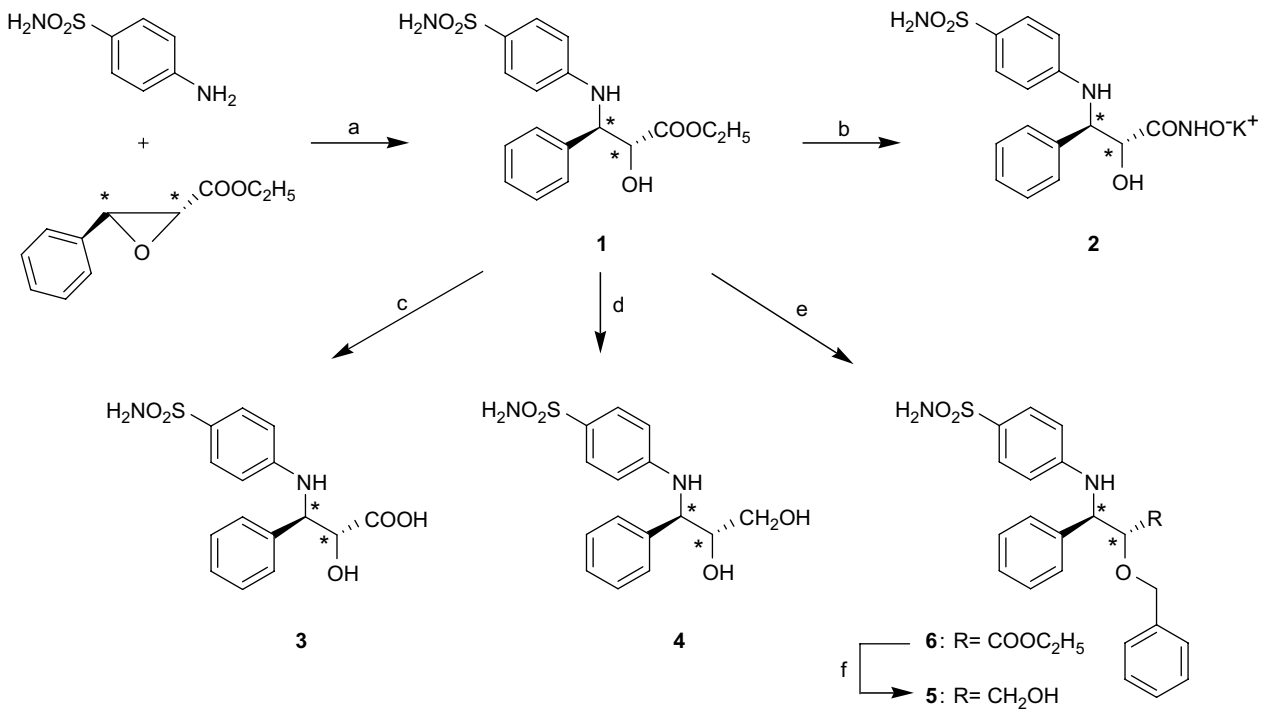

Scheme 1. Reagents and conditions: (a) $CoCl_2$, NMP, MeCN; (b) 1 M NH_2OH, MeOH–KOH; (c) 1.6 N NaOH, 95% EtOH; (d) 2 M $LiBH_4$, THF, N_2; (e) $C_6H_5CH_2Br$, K_2CO_3, THF; (f) 2 M $LiBH_4$, THF, N_2.

[8]. Both active sites form a cone where the catalytic zinc ion, coordinated to three histidine residues, constitutes the summit. Hydrophilic and hydrophobic subsites are located on either side of the zinc coordination site which establishes the main interaction with carbonic anhydrase inhibitors by complexation with a sulfonamide moiety.

So as to understand why replacing the primary alcohol function (**4**) by a carboxylic group (**3**) led to better selectivity towards hCA IX (Table 1), we used docking studies to specify the binding mode of the selective hCA IX inhibitor **3** and the hCA II selective inhibitor **4**. *R*,*R* and *S*,*S* enantiomers were considered for each compound binding mode inside the respective active sites of hCA IX and hCA II isozymes.

Table 1
Inhibition and selectivity ratio data for AZA and compounds **1**–**5** towards isozymes hCA I, hCA II and hCA IX

Compound	K_I (nM)[a]			K_I ratios[b]	
	hCA I	hCA II	hCA IX	hCA I/hCA IX	hCA II/hCA IX
AZA	900	12	25	36	0.5
1	8386	49	27	311	1.8
2	62	1.4	2.3	27	0.6
3	707	17	1.8	393	9.4
4	235	8.1	18	13	0.4
5	221	91	227	1.0	0.4

[a] Errors were in the range of 3–5% of the reported values, from three different assays.

[b] The K_I ratios are indicative of inhibition selectivity: a weak selective inhibitor is characterized by a low value ratio.

*2.3.1. Docking of compound **3** inside both hCA II and hCA IX*

These dockings are illustrated in Fig. 1A and B, respectively. Firstly, analysis of the binding mode of **3** within hCA II showed, on the one hand, that enantiomer *R*,*R* (colored in blue) anchors its unsubstituted phenyl ring in a pocket delimited by aromatic residues His93, His95, His63 and Trp4 and makes H bonds with Asn61, Asn66 and Gln91 residues. We called this specific binding mode the "ARO" mode. On the other hand, two conformations (colored in orange and in yellow) were observed for enantiomer *S*,*S*. In the orange conformation, the phenyl ring was oriented within the aromatic pocket of hCA II (binding mode 2, ARO mode). In the yellow conformation, the enantiomer *S*,*S* made a π–π T-shaped interaction between its phenyl ring and the Phe129 hCA II-specific residue. This binding mode was called binding mode 1, "PHOBIC" mode. In this orientation, one H bond was found between the carbonyl moiety and Gln91. As previously described [8], the sulfonamide group was anchored at the zinc coordination site level. This interaction represents the main contribution to the interaction energies that have been computed for each binding mode: no discrimination can be made between either binding mode ("ARO" or "PHOBIC") of enantiomer *S*,*S*, as both are in the same range of interaction energies (Table 2).

Secondly, the binding mode of both enantiomers of inhibitor **3** within hCA IX was of the "ARO" type. The aromatic pocket of the hCA IX active site was delimited by His226, His228, His200 and Trp141. Each enantiomer fitted its phenyl ring in the same aromatic pocket but adopted a different

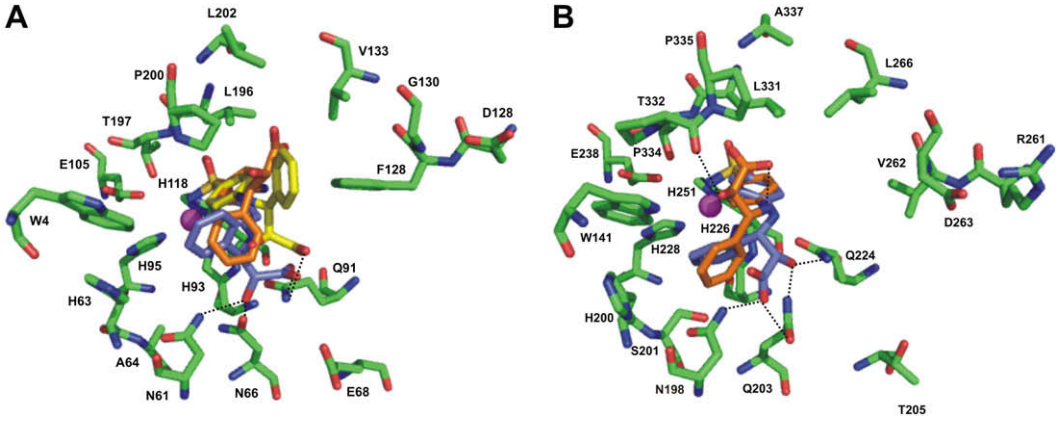

Fig. 1. A) Binding modes of compound **3** in the hCA II active site. Enantiomer *R*,*R* (colored in blue) forms H bonds (as black mark) with Asn61, Asn66 and Gln91. Enantiomer *S*,*S* fits the hCA II according to two binding modes: the first mode (in yellow, binding mode 1, ''PHOBIC'' mode) positions its phenyl ring to interact by π–π contact with Phe129. H bond is found between the carbonyl moiety and Gln91. In the second mode (in orange, binding mode 2, ''ARO'' mode) there is no H bond but its phenyl ring fits in the aromatic pocket, as does enantiomer *R*,*R*. (B) Docking of enantiomers *R*,*R* (in orange) and *S*,*S* **3** (in blue) in the hCA IX active site. Each enantiomer has the same binding mode for the phenyl ring but differs as to the position of the side chain. Enantiomer *R*,*R* establishes H bond with Pro334 and an intramolecular H bond. Enantiomer *S*,*S* interacts by H bonds with Gln224, Gln203 and Asn198.

conformation inside the hCA IX site at the flexible side chain level (Fig. 1B). The computed interaction energies of each enantiomer in hCA IX showed that enantiomer *S*,*S* was stabilized by about 4 kcal mol^{-1} (Table 2). This slight decrease in energy can be explained by the improved fit of the phenyl moiety inside the aromatic pocket and by the presence of several H bonds between the inhibitor side chain and amino acids of the hydrophilic pocket.

2.3.2. Docking of compound 4 inside both hCA II and hCA IX

These dockings are illustrated in Fig. 2A and B, respectively. Two main binding modes (named 1 and 2) were observed between hCA II and each enantiomer of compound **4**, whereas only one binding mode was noted for the hCA IX active site. Nevertheless, the general ligand conformation was similar within the two isoforms. It is interesting to note that the unsubstituted phenyl ring fitted the aromatic pocket perfectly in the hCA II active site (Fig. 2A). The unique difference between the several binding modes is to be found at the flexible hydroxymethyl side chain level. According to its orientation, the alcohol moiety can establish H bonds with several amino acid residues. In the case of hCA II, a strong H bond interaction was detected between the alcohol moiety of enantiomer *R*,*R* (in cyan, Fig. 2A) and Glu68, a specific amino acid of hCA II. This may partially explain the better inhibitory activity of compound **4** towards hCA II vs. hCA IX (Table 1).

In the case of hCA IX (Fig. 2B), we noted that enantiomer *R*,*R* orients its phenyl moiety slightly outside the aromatic pocket: this additional feature may contribute to a decrease in the inhibitory activity of compound **4** towards hCA IX.

These docking studies helped us to understand and rationalize the enzymatic activity of inhibitors **3** and **4**. Compound **3** exhibited better inhibition activity than compound **4** towards hCA IX, which can be explained by the formation of more H bonds between **3** and hCA IX residues. On the contrary, however, the inhibitory activity of compound **4** towards hCA II was better than that of compound **3** (8.1 nM vs.17 nM). Two features were highlighted and could contribute to a decrease in inhibitory potency: (i) each conformation of compound **4** perfectly fits its phenyl moiety within the aromatic pocket while the phenyl ring of compound **3** adopts two different conformations, (ii) a strong H bond is observed for one binding mode between the primary alcohol of compound **4** and Glu68, a specific residue only present in hCA II.

Docking studies of compounds **3** and **4** highlighted an additional pocket present in both isozymes which has never been described before. This aromatic pocket was also observed [14] by an aromatic GRID probe in hCA II and in hCA IX (Fig. 3). From these findings, a two-dimensional schematic view of the hCA II and hCA IX active sites can be drawn (Fig. 4). Although their topology was well preserved, we noted that the hydrophobic subsite was smaller in hCA II

Table 2
Interaction energies[a] for compounds **3** and **4** with hCA II and hCA IX isozymes

Compound	Enzyme	Enantiomer (binding mode)	Phenyl position	ΔE_{Cb}	ΔE_{vdW}	ΔE_{tot}
3	hCA II	*R*,*R*	ARO	−35.0	−9.3	−44.3
3	hCA II	*S*,*S* (1)	PHOBIC	−31.3	−12.2	−43.6
3	hCA II	*S*,*S* (2)	ARO	−26.5	−13.5	−40.0
3	hCA IX	*R*,*R*	ARO	−31.2	−13.7	−44.9
3	hCA IX	*S*,*S*	ARO	−39.3	−9.7	−49.0
4	hCA II	*R*,*R* (1)	ARO	−26.0	−15.2	−41.2
4	hCA II	*R*,*R* (2)	ARO	−29.0	−14.1	−43.1
4	hCA II	*S*,*S* (1)	ARO	−23.6	−15.6	−39.2
4	hCA II	*S*,*S* (2)	ARO	−27.3	−15.8	−43.2
4	hCA IX	*R*,*R*	ARO	−27.9	−10.6	−38.5
4	hCA IX	*S*,*S*	ARO	−27.3	−12.8	−40.1

[a] All energies are expressed in kcal mol^{-1}. Total interaction energy (ΔE_{tot}) is computed as the sum of van der Waals (vdW) and Coulombic (Cb) contributions. ''ARO'' mode corresponds to the fitting of the phenyl ring in the aromatic pocket. In the ''PHOBIC'' binding mode, the phenyl ring interacts with the Phe residue present in the hydrophobic pocket of hCA II.

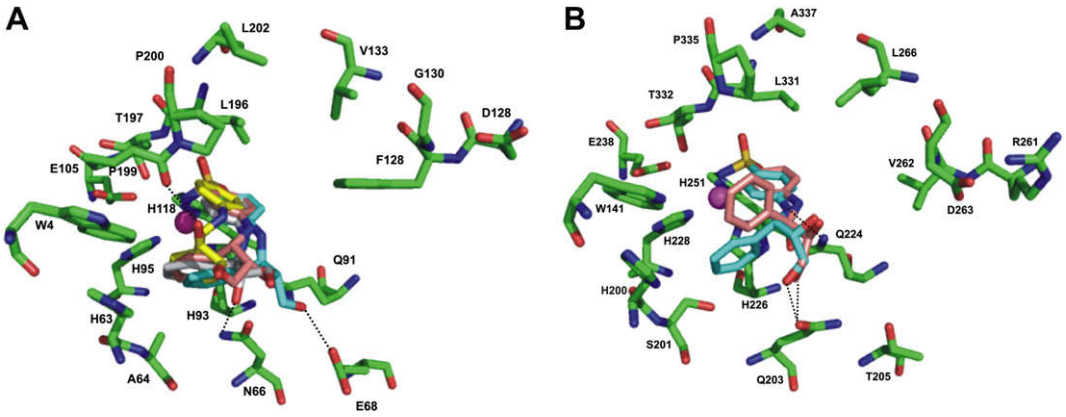

Fig. 2. (A) Docking of compound **4** inside the hCA II active site. The phenyl ring is anchored in the aromatic pocket while the side chain exhibits several possible binding modes. Enantiomer *R*,*R* can adopt two different conformations within the active site (colored in light grey and in cyan). In the first conformation (light grey, binding mode 1), H bond is observed with Asn66 while in the second one (cyan, binding mode 2) H bond is formed with Glu68. Two binding modes have also been found for enantiomer *S*,*S* (colored in pink, binding mode 1 and in yellow, binding mode 2): the yellow one shows an interaction with Pro199. (B) Docking of compound **4** inside the hCA IX active site. Enantiomer *R*,*R* is colored in pink and enantiomer *S*,*S* is colored in cyan. H bonds are observed between enantiomer *R*,*R* and Gln203, Gln224. Enantiomer *S*,*S* makes H bonds with Gln203 and Gln224.

than in hCA IX, because of the mutation of Phe129 in hCA II into Asp263 in hCA IX. In both cases, the aromatic pocket was surrounded by three histidine and one tryptophan residues but the hCA II pocket was more restrained than that of hCA IX. Several differences could be observed between the hydrophilic pocket of the two isoforms: Ala64, Asn66 and Glu68, present in hCA II, were replaced by Ser201, Gln203 and Thr205 in hCA IX [8]. Globally, the active site of hCA II was more restricted than the active site of hCA IX, as assessed by the solvent accessible area calculation (731 $Å^2$ for hCA II and 909 $Å^2$ for hCA IX) [15,16].

3. Conclusions

We report in this paper the synthesis and biological evaluation of new benzylanilinosulfonamides as hCA inhibitors synthesized through a regio- and stereoselective procedure. Their inhibition activity was determined towards two biologically relevant CA isozymes (hCA I and hCA II) and towards hCA IX, which has been found to play a role in cancer. The presence of two aryl moieties spaced by three covalent bonds, never previously described for hCA inhibitors, confers interesting inhibitory properties to these compounds. Compound **3** was found to be particularly active and selective towards the tumor-associated hCA IX. A molecular modeling study was performed to simulate the binding modes of compounds **3** and **4** – selective hCA IX and hCA II inhibitors, respectively – and to rationalize their enzymatic activities. In addition to the already described hydrophobic and hydrophilic subsites [3,6,8], an additional pocket delimited by aromatic amino acid residues present in the active site of both isoforms was highlighted.

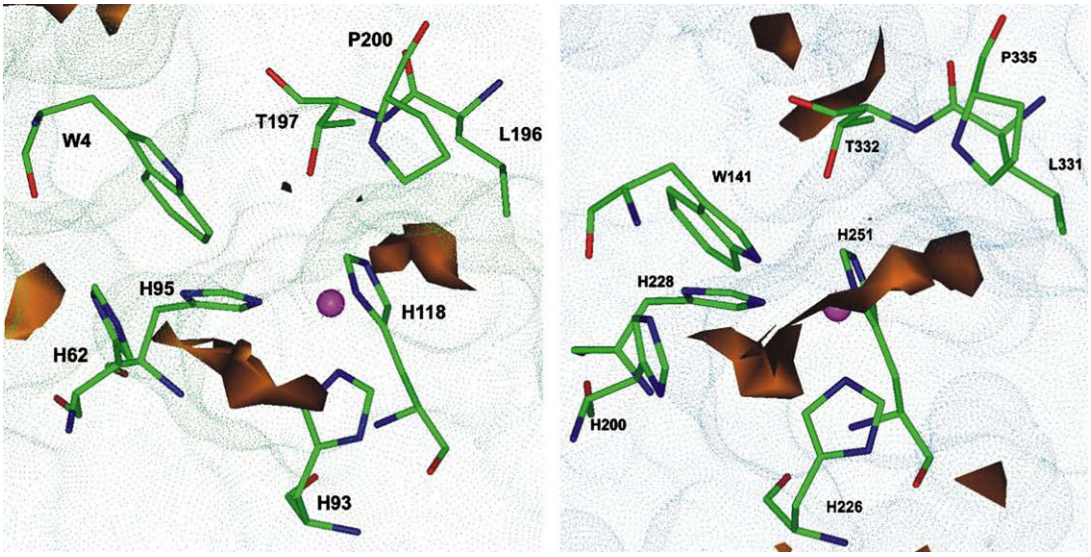

Fig. 3. Zoom of the hCA II (left) and the hCA IX (right) active sites at the zinc coordinated level with the aromatic GRID probe (colored in orange) and their Connolly surface (probe 1.4 Å) defining the accessible binding pocket.

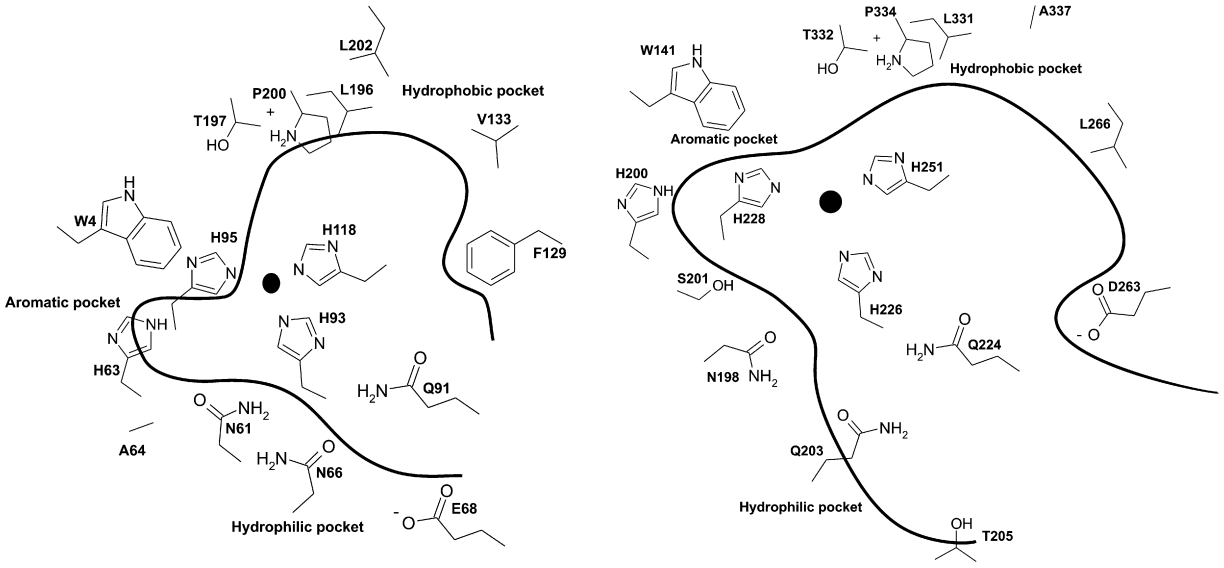

Fig. 4. Schematic representation of the hCA II (left) and hCA IX (right) active sites. hCA II active site is more restricted than the active site of hCA IX as assessed by the solvent accessible area calculation (731 $Å^2$ for hCA II and 909 $Å^2$ for hCA IX).

In view of these original findings, synthesis of additional molecules is warranted and particular attention should be paid to the removal of the two chiral centers. Consequently, more restrained derivatives possessing this original benzylanilinosulfonamide scaffold should be designed in an attempt to confirm the anchoring of the additional phenyl ring in the aromatic pocket. It would also clarify the structure–activity relationships within this new family.

4. Experimental

4.1. Chemistry

Unless otherwise noted, moisture-sensitive reactions were performed under dry nitrogen. Tetrahydrofuran was distilled from sodium/benzophenone prior to use. Flash chromatography (FC) was performed with silica gel Kieselgel Si 60, 0.040–0.063 mm (Merck). Melting points were determined with a Büchi 535 capillary melting point apparatus and are uncorrected. The structure of each compound was confirmed by IR (neat, FT-Bruker Vector 22 instrument), by ^{1}H NMR (300 MHz, Bruker DPX-300 spectrometer) and by ^{13}C NMR (75 MHz, Bruker AC-300 spectrometer). Chemicals shifts (δ) are reported in ppm downfield from TMS, J values are in Hertz, and the splitting patterns are designed as follows: s, singlet; d, doublet; t, triplet; m multiplet; br s, broad singlet. APCI$^+$ (atmospheric pressure chemical ionization) mass spectra were obtained on an LC–MS system Thermo Electron Surveyor MSQ. Elemental analyses were performed by the ''Service Central d'Analyses'' at the CNRS, Vernaison, France.

4.1.1. Ethyl (2R,3R*)-anti-3-[4-(aminosulfonyl)anilino]-2-hydroxy-3-phenylpropanoate (**1**)*

Ethyl *trans*-phenylglycidate (22 mL, 128 mmol) was diluted in a solution of NMP (1 mL) in acetonitrile (200 mL), then 4-aminobenzenesulfonamide (11 g, 64 mmol) and dry cobalt(II) chloride (5 mol%, 830 mg) were added. The resulting mixture was refluxed for 3 days in a dry nitrogen atmosphere. After removal of the solvent, the residue was dissolved in EtOAc (100 mL) and successively washed with a saturated solution of $NaHCO_3$, with 1 N HCl and brine. The organic layer was dried ($MgSO_4$), and the solvent was removed under reduced pressure. The residue was purified by FC (heptane/EtOAc 1:1) and recrystallized in toluene to give ester **1** as a white solid; yield: 56%; m.p. 60–61 °C; IR ν_{max}: 3384 (OH), 3264 (NH), 1732 (C=O), 1598 (C=C), 1153 (SO_2) cm^{-1}; ^{1}H NMR ($CDCl_3$) δ 7.61 (d, $J = 8.4$, 2H), 7.27 (m, 5H), 6.58 (d, $J = 8.4$, 2H), 5.51 (br s, 1H), 4.88 (d, $J = 3.2$, 1H), 4.76 (br s, 2H), 4.68 (d, $J = 3.2$, 1H), 4.21 (m, 2H), 1.66 (br s, 1H), 1.29 (t, $J = 7.1$, 3H); ^{13}C NMR (DMSO-d_6): δ 14.5, 59.1, 60.4, 73.9, 112.8, 127.1, 127.2, 128.8, 128.9, 131.7, 140.1, 150.5, 172.9; LC–MS (APCI$^+$) m/z 365 (MH$^+$). Anal. ($C_{17}H_{20}N_2O_5S$) C, H, N.

4.1.2. (2R,3R*)-anti-3-[4-(Aminosulfonyl)anilino]-2-hydroxy-3-phenylpropanoic acid hydroxyamide potassium salt (**2**)*

1 M NH_2OH/MeOH–KOH was prepared from a solution of $NH_2OH \cdot HCl$ (2.88 g, 41 mmol) in MeOH (25 mL) added to a solution of KOH (2.88 g, 51 mmol) in MeOH (13 mL) before KCl was filtered off. NH_2OH (1 M in MeOH–KOH, 20 mL) was added to ester **1** (0.6 g, 2.1 mmol) at 4 °C. The reaction mixture was stirred for 4 h at room temperature. The precipitate was collected by filtration and washed with MeOH (3×100 mL) to give hydroxamate **2**; yield: 40%; m.p. 186–188 °C; IR ν_{max}: 3338 (NH), 1677 (C=O), 1603 (C=C), 1312 (SO_2), 1152 (SO_2) cm^{-1}; ^{1}H NMR (DMSO-d_6) δ 7.05–7.70 (m, 9H), 6.51 (d, $J = 8.1$, 2H), 4.55 (br s, 1H), 3.93 (br s, 1H), 3.37 (br s, 1H); ^{13}C NMR (DMSO-d_6): δ 60.8, 73.8, 112.2, 127.7, 127.8, 128.0, 128.1, 130.2, 140.1,

151.1, 137.1; LC–MS (APCI$^+$) *m/z* 352 (MH^+). Anal. ($C_{15}H_{16}KN_3O_5S \cdot H_2O$) C, H, N.

4.1.3. (2R*,3R*)-anti-3-[4-(Aminosulfonyl)anilino]-2-hydroxy-3-phenylpropanoic acid (3)

Ester **1** (0.5 g, 1.4 mmol) was dissolved in 95% EtOH (30 mL), 1.6 N NaOH (10 mL) was added and the solution was stirred for 3 h. The solvents were evaporated under reduced pressure. The aqueous layer was washed with CH_2Cl_2 (2 × 10 mL), then acidified with 1 N HCl. The resultant precipitate was collected by filtration and recrystallized in a mixture of toluene and acetonitrile to give carboxylic acid **3** as a white solid; yield: 62%; m.p. 157–158 °C; IR ν_{max}: 3517 (OH), 3428 (OH), 3311 (NH), 1718 (C=O), 1307 (SO_2), 1138 (SO_2) cm^{-1}; ^1H NMR (DMSO-d_6) δ 12.71 (br s, 1H), 7.24–7.44 (m, 7H), 6.89 (br s, 2H), 6.68 (d, $J = 8.4$, 2H), 5.68 (br s, 1H), 4.76 (m, 1H), 4.30 (d, $J = 6.1$, 1H), 3.37 (br s, 1H); ^{13}C NMR (DMSO-d_6): δ 58.5, 74.2, 112.5, 127.4, 127.5, 128.7, 128.9, 130.9, 139.5, 150.4, 174.4; LC–MS (APCI$^+$) *m/z* 337 (MH^+). Anal. ($C_{15}H_{16}N_2O_5S \cdot 0.5H_2O$) C, H, N.

4.1.4. (1R*,2R*)-anti-4-[(2,3-Dihydroxy-1-phenylpropyl)amino]-1-benzenesulfonamide (4)

Ester **1** (5 g, 14 mmol) was dissolved at 0 °C in dry THF (150 mL) in a nitrogen atmosphere before adding $LiBH_4$ (2 M in THF, 10.5 mL, 21 mmol). The mixture was stirred for 3 h at room temperature, then 0.5 N HCl (30 mL) was added and further stirred for an additional 1 h. The precipitated white solid was filtered off, washed with water and recrystallized in isopropanol to give alcohol **4** as a white solid; yield: 82%; m.p. 198–199 °C; IR ν_{max}: 3503 (OH), 3486 (OH), 3355 (NH), 1598 (C=C), 1311 (SO_2), 1137 (SO_2) cm^{-1}; ^1H NMR (DMSO-d_6) δ 7.38 (m, 4H), 7.27 (d, $J = 6.5$, 2H), 7.19 (t, $J = 6.5$, 1H), 6.82 (br s, 2H), 6.59 (d, $J = 8.5$, 2H), 4.87 (br s, 1H), 4.72 (br s, 1H), 4.53 (m, 1H), 3.83 (m, 1H), 3.32 (m, 2H); ^{13}C NMR (DMSO-d_6): δ 58.3, 63.3, 74.3, 112.7, 127.5, 127.6, 127.8, 127.9, 130.7, 140.6, 150.6; LC–MS (APCI$^+$) *m/z* 323 (MH^+). Anal. ($C_{15}H_{18}N_2O_4S$) C, H, N.

4.1.5. Ethyl (2R*,3R*)-anti-3-[4-(aminosulfonyl)anilino]-2-benzyloxy-3-phenylpropanoate (6)

A solution of ester **1** (1 g, 2.7 mmol) in THF (100 mL) was stirred while potassium carbonate (2.2 g, 16 mmol) was added rapidly at room temperature before benzyl bromide (1 mL, 8.2 mmol) was added in one batch. The reaction mixture was stirred for 15 h at 70 °C, then concentrated under reduced pressure, and the residue extracted with EtOAc. The organic layer was washed with water, brine, dried ($MgSO_4$), and concentrated under reduced pressure. The crude product was purified by FC (heptane/EtOAc 65:35) to give ester **6** as a white solid; yield: 50%; IR ν_{max}: 2970 (NH), 2924 (NH), 1731 (C=O), 1596 (C=C), 1303 (SO_2), 1149 (SO_2) cm^{-1}; ^1H NMR ($CDCl_3 + D_2O$) δ 7.61 (d, $J = 8.7$, 2H), 7.23 (m, 10H), 6.79 (d, $J = 8.7$, 2H), 4.90 (d, $J = 3.3$, 1H), 4.69 (d, $J = 3.3$, 1H), 4.68 (m, 2H), 4.06 (m, 2H), 1.29 (m, 3H).

4.1.6. (1R*,2R*)-anti-4-{[2-(Benzyloxy)-3-hydroxy-1-phenylpropyl]amino}benzenesulfonamide (5)

Ester **6** (0.5 g, 1.1 mmol) was dissolved in THF (50 mL) in dry nitrogen atmosphere, then $LiBH_4$ (2 M in THF, 1.7 mL, 3.3 mmol) was added. The solution was stirred for 3 h at room temperature. The reaction mixture was concentrated under reduced pressure, and the crude residue was diluted in EtOAc. The precipitated white solid was filtered off and washed with EtOAc (2 × 20 mL). The organic layer was collected, washed with brine (2 × 20 mL), dried ($MgSO_4$) and the solvent was removed under reduced pressure. The crude material was purified by recrystallization (CH_2Cl_2) to give benzyl ether **5** as a white solid; yield: 72%; m.p. 104–105 °C; IR ν_{max}: 3348 (OH), 1596 (C=C), 1308 (SO_2), 1148 (SO_2) cm^{-1}; ^1H NMR ($CDCl_3$) δ 7.57 (d, $J = 8.5$, 2H), 7.39–7.18 (m, 10H), 6.57 (d, $J = 8.5$, 2H), 5.67 (br s, 1H), 4.70 (m, 1H), 4.44 (br s, 1H), 4.06 (m, 3H), 3.65 (m, 2H); ^{13}C NMR (DMSO-d_6): δ 46.3, 58.7, 62.8, 74.3, 112.2, 127.1, 127.2, 128.2, 128.3, 128.6, 128.7, 138.3, 141.4, 151.9; LC–MS (APCI$^+$) *m/z* 413 (MH^+). Anal. ($C_{22}H_{24}N_2O_4S$) C, H, N.

4.2. CA inhibition

hCA I and hCA II were supplied by Sigma–Aldrich. The recombinant hCA IX enzyme was obtained as reported earlier [17]. An SX.18MV-R Applied Photophysics stopped-flow instrument was used for the CA CO_2 hydration activity assays [18]. Phenol red (at a concentration of 0.2 mM) was used as indicator, with 10 mM HEPES (pH 7.5) as buffer and 0.1 M Na_2SO_4 to make ionic strength constant. The CA-catalyzed CO_2 hydration reaction was followed for a period of 10–100 s, working at maximum absorbance wavelength of 557 nM. A saturated CO_2–water solution at 20 °C was used as substrate. Stock solutions of each inhibitor (1 mM) were prepared in distilled-deionized water with 10–20% (v/v) DMSO (which does not influence measures at these concentrations) whereas dilutions of up to 0.1 nM were thereafter prepared with distilled-deionized water. To allow for the formation of the E–I complex, solutions of inhibitor and enzyme were preincubated for 15 min at room temperature prior to assay. The inhibition constants were obtained by nonlinear least-squares methods using PRISM3. The curve-fitting algorithm allowed us to obtain the IC_{50} values from which the K_I values were calculated by using the Cheng–Prusoff equation. The catalytic activity (in the absence of inhibitors) of these enzymes was calculated form Lineweaver–Burk plots, as reported earlier [19,20]. Enzyme concentrations were 1.0 μM for hCA I and hCA II and 0.1 μM for hCA IX. Each experiment was performed in triplicate.

4.3. Molecular modeling

All computational experiments were conducted on a Silicon Graphics Octane2 workstation, running the IRIX 6.5 operating system. Molecular modeling studies were carried out

using InsightII software (version 2005) [21]. Inhibitor structures were constructed using the BUILDER module implemented in InsightII and optimized with the CFF91 force field. The carboxylic moiety of compound **3** was modeled in its deprotonated form. Docking studies were performed inside the hCA IX model [8] and inside the experimental crystal structure of hCA II (PDB entry: 1A42) [22] with the genetic algorithm GOLD (version 3.0) [23]. GOLD performs docking of flexible ligands into protein with partial flexibility in the neighbourhood of the active site (Ser, Thr, Tyr and Lys). Default settings were used for genetic algorithm parameters. The interaction sphere was centered on the zinc of the active site and delimited by a 12 Å radius. A tetrahedral geometry was imposed on the zinc binding site. Thirty solutions were generated and ranked according to the GOLD score. Only the most frequent binding mode with the highest GOLD score was considered. To assess protein flexibility, the DISCOVER3 program [24], from InsightII software [21], was used to refine the complexes (ESFF force field and dielectric constant $= 1 \times r$). The energetic minimization process was performed in two steps: the Steepest Descent algorithm to reach a convergence of 10 kcal mol^{-1} $Å^{-1}$, followed by the Conjugate gradient to reach a final convergence of 0.01 kcal mol^{-1} $Å^{-1}$. First, all the protein atoms were held fixed and only the orientation of the ligand was optimized. Then the side chains of active site residues followed by their backbone were relaxed. A tethering restraint was applied to these atoms to keep them from moving too far from their original positions. This restraint had a quadratic form with a constant force of 10 kcal $Å^{-2}$ and was progressively decreased (scale factor of 0.5).

The active site was explored with an aromatic GRID probe (version 2.2) [14]. The contour maps were visualized using the contour facility of InsightII. Calculations were made with a grid spacing of 1.0 Å. Interaction energy between the probe and every atom within the protein structure was evaluated at each grid point.

The solvent accessible area was calculated using Naccess software [15,16]. In our case, data were compiled over the hCA II or hCA IX active site residues. Naccess calculated the atomic area with a probe rolled around the van der Waals surface of the macromolecule.

Figs. 1 and 2 were produced by PyMOL [25].

Acknowledgments

A. Thiry is greatly indebted to the "Fonds de la Recherche Scientifique (F.R.S.-FNRS)" for the award of a research fellowship. This work was partly supported by a grant from the "Fonds pour la Recherche Scientifique Médicale" (FRSM).

References

[1] S. Pastoreková, S. Parkkila, J. Zavada, Adv. Clin. Chem. 42 (2006) 167–216.
[2] A. Thiry, J.-M. Dogné, B. Masereel, C.T. Supuran, Trends Pharmacol. Sci. 27 (2006) 566–573.
[3] C.T. Supuran, A. Casini, A. Scozzafava, in: C.T. Supuran, A. Casini, J. Conway (Eds.), Development of Sulfonamide Carbonic Anhydrase Inhibitors, CRC Press, Boca Raton, FL, 2004, pp. 67–147.
[4] C.T. Supuran, A. Scozzafava, A. Casini, Med. Res. Rev. 23 (2003) 146–189.
[5] A. Thiry, J.-M. Dogné, C.T. Supuran, B. Masereel, Curr. Top. Med. Chem. 7 (2007) 855–864.
[6] C.T. Supuran, Curr. Top. Med. Chem. 7 (2007) 825–833.
[7] C.T. Supuran, A. Scozzafava, Bioorg. Med. Chem. 15 (2007) 4336–4350.
[8] A. Thiry, M. Ledecq, A. Cecchi, J.-M. Dogné, J. Wouters, C.T. Supuran, B. Masereel, J. Med. Chem. 49 (2006) 2743–2749.
[9] M. Chini, P. Crotti, L.A. Flippin, F. Macchia, J. Org. Chem. 56 (1991) 7043–7048.
[10] J. Iqbal, A. Pandey, Tetrahedron Lett. 31 (1990) 575–576.
[11] B. Bhatia, S. Jain, A. De, I. Bagchi, J. Iqbal, Tetrahedron Lett. 37 (1996) 7311–7314.
[12] A. De, S. Ghosh, J. Iqbal, Tetrahedron Lett. 38 (1997) 8379–8382.
[13] S. Odake, K. Nakahashi, T. Morikawa, S. Takebe, K. Kobashi, Chem. Pharm. Bull. 40 (1992) 2764–2768.
[14] P.J. Goodford, J. Med. Chem. 28 (1985) 849–857.
[15] S.J. Hubbard, J. Thornton, Naccess, Version 2.1.1, 1996.
[16] B. Lee, F.M. Richards, J. Mol. Biol. 55 (1971) 379–400.
[17] D. Vullo, M. Franchi, E. Gallori, J. Antel, A. Scozzafava, C.T. Supuran, J. Med. Chem. 47 (2004) 1272–1279.
[18] R.G. Khalifah, J. Biol. Chem. 246 (1971) 2561–2573.
[19] J.Y. Winum, D. Vullo, A. Casini, J.L. Montero, A. Scozzafava, C.T. Supuran, J. Med. Chem. 46 (2003) 5471–5477.
[20] J.Y. Winum, D. Vullo, A. Casini, J.L. Montero, A. Scozzafava, C.T. Supuran, J. Med. Chem. 46 (2003) 2197–2204.
[21] Accelrys, InsightII, Version 2005, San Diego, CA, 2005.
[22] T. Stams, Y. Chen, P.A. Boriack-Sjodin, J.D. Hurt, J. Liao, J.A. May, T. Dean, P. Laipis, D.N. Silverman, D.W. Christianson, Protein Sci. 7 (1998) 556–563.
[23] G. Jones, P. Willett, R.C. Glen, A.R. Leach, R. Taylor, J. Mol. Biol. 267 (1997) 727–748.
[24] Accelrys, Discover3, Version 2.98, San Diego, CA, 1998.
[25] W.L. DeLano, The PyMOL Molecular Graphics System, DeLano Scientific, Palo Alto, CA, USA, 2002.